

Supplementary Information

Dual-Fibrous PTFE Structure Enabling Uniform and Thick Dry Electrodes for High-Energy-Density and Long-Lasting Batteries

Kwon-Hyung Lee^{a,c,†}, Hyeongseok Shim^{a,d,†}, Sang Hyun Lee^a, Hyeong-Jong Kim^e, Chanhyun Park^e, Jingyu Choi^e, Seok-Ju Lee^f, Young-Kuk Hong^f, Jihong Lyu^g, Jin Chul Kim^g, Sijeong Park^{a,e}, Hyungyeon Cha^a, Wooyoung Jin^a, Jinsoo Kim^h, Sinho Choi^a, Sang-Young Lee^f, Sung-Kyun Jung^{i,j,k,l}, Michael De Volder^c, Tae-Hee Kim^{b*}, Gyujin Song^{a*}

^aUlsan Advanced Energy Technology R&D Center, Korea Institute of Energy Research (KIER), Ulsan 44776, Republic of Korea

^bSchool of Chemical Engineering, University of Ulsan, Ulsan 44610, Republic of Korea

^cDepartment of Engineering, University of Cambridge, Cambridge, CB3 0FS, United Kingdom

^dSchool of Materials Science and Engineering, Kyungpook National University, Daegu, 41566, Republic of Korea

^eSchool of Energy and Chemical Engineering, Ulsan National Institute of Science and Technology (UNIST), Ulsan 44919, Republic of Korea

^fDepartment of Chemical and Biomolecular Engineering, Yonsei University, Seoul 03722, Republic of Korea

^gDepartment of Specialty Chemicals, Division of Specialty and Bio-based Chemicals Technology, Korea Research Institute of Chemical Technology (KRICT), Ulsan 44412, Republic of Korea

^hDepartment of Energy Science and Engineering, Daegu Gyeongbuk Institute of Science and Technology (DGIST), Daegu 42988, Republic of Korea

ⁱResearch Institute of Advanced Materials (RIAM), Seoul National University (SNU), Seoul 08826, Republic of Korea

^jSchool of Transdisciplinary Innovations, Seoul National University (SNU), Seoul 08826, Republic of Korea

^kDepartment of Materials Science and Engineering, Seoul National University (SNU), Seoul 08826, Republic of Korea

^lInstitute for Rechargeable Battery Innovations Research, Seoul National University (SNU), Seoul 08826, Republic of Korea

[†]These authors contributed equally to this work

*Correspondence: gyujin.song@kier.re.kr (G.S.), kimtaehee@ulsan.ac.kr (T.-H.K.)

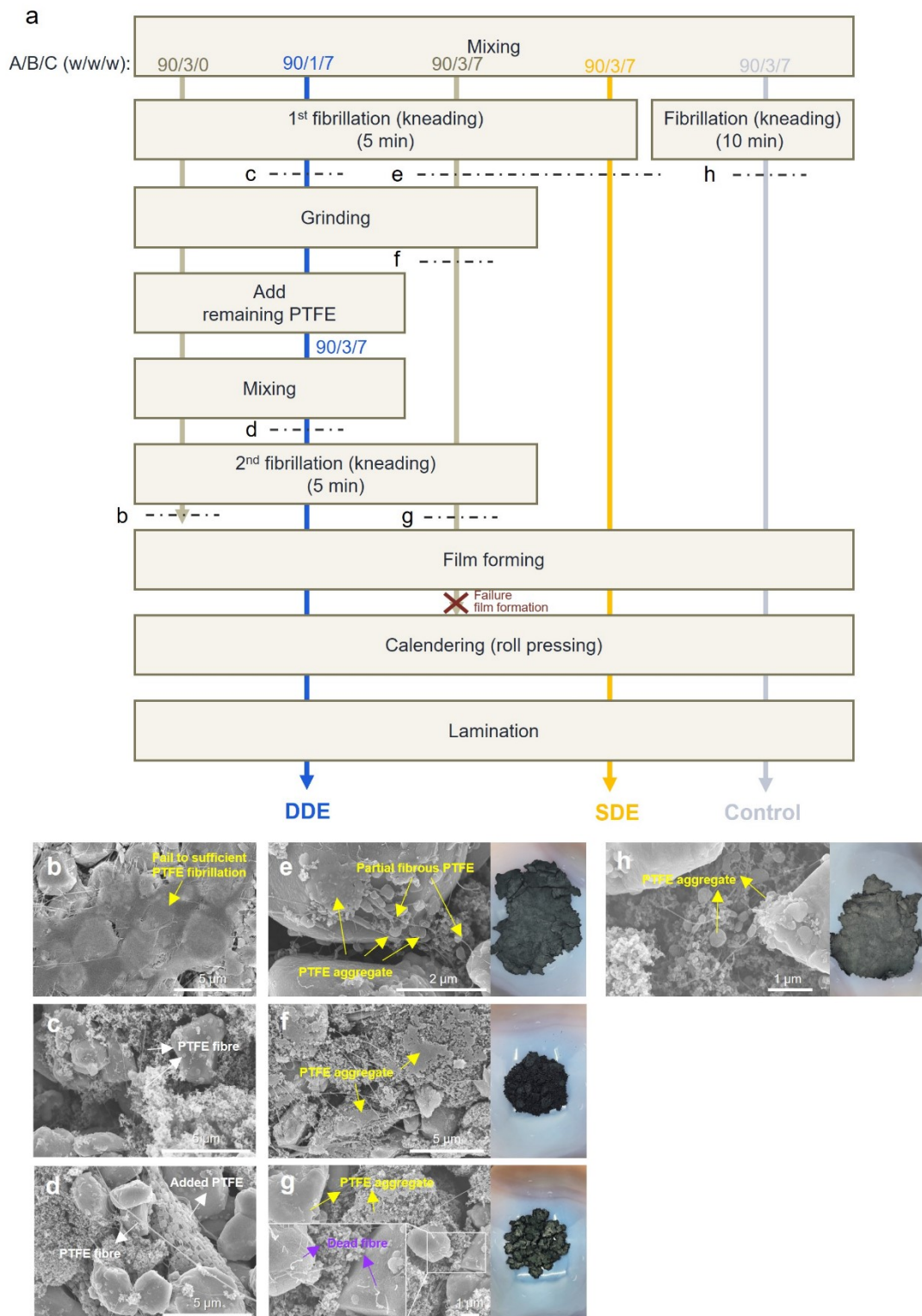


Figure S1. (a) A flowchart representing electrode fabrication of DDE, SDE and control samples. (b-g) Corresponding SEM (or with photograph images) of electrode powder at various stage: (b) After second kneading without CB (i.e., A/B/C = 90/3/0 (w/w/w)) (c) After first kneading of DDE, (d) after grinding and mixing with an additional 2 wt% of PTFE in the DDE, (e) after first kneading of SDE, (f) after grinding and (g) second kneading of the control sample (h) after extended first kneading (10 min) of control sample without grinding.

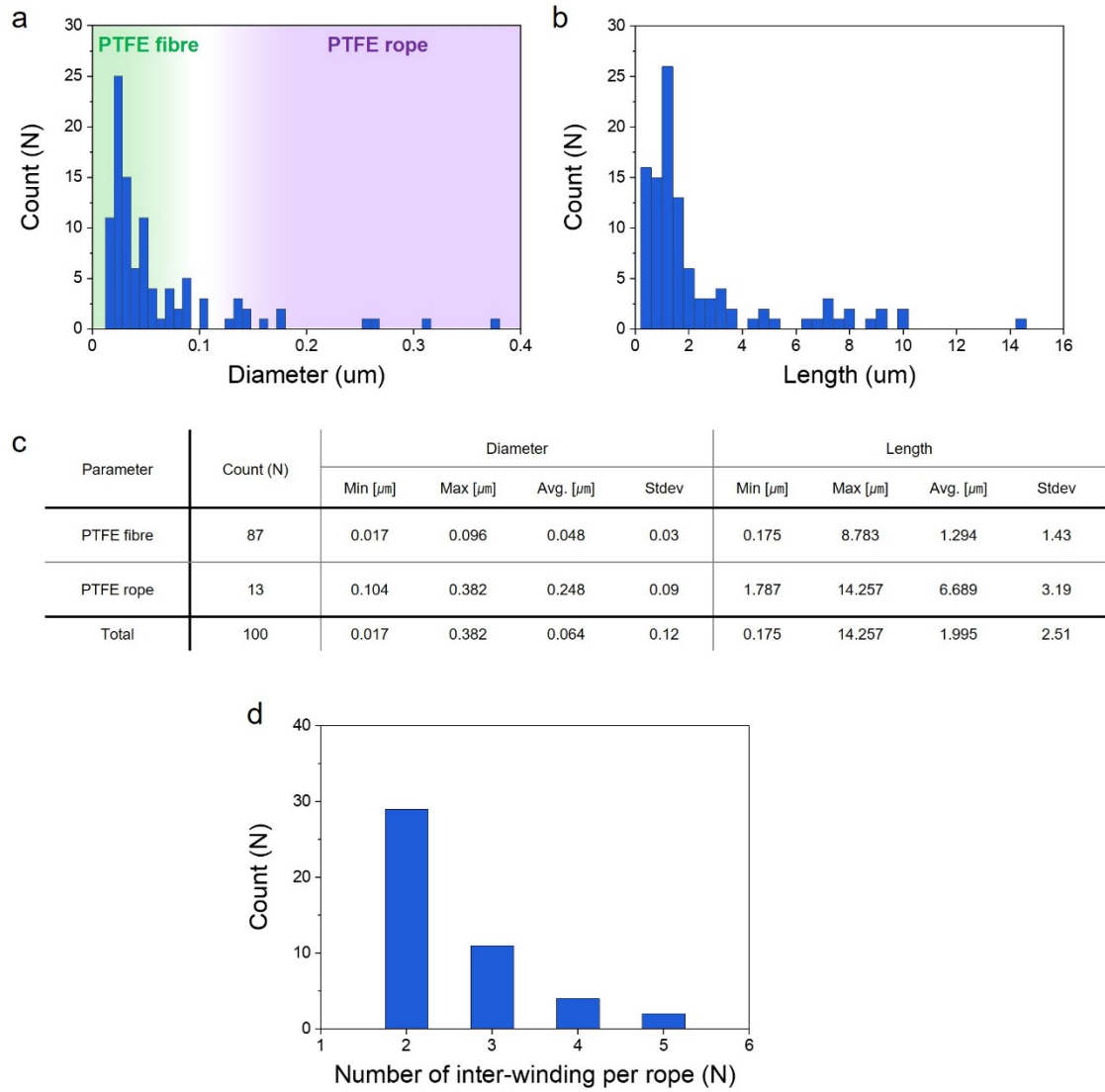


Figure S2. Quantitative characterisation of PTFE fibres and ropes. Distribution of (a) diameter and (b) length. (c) Summary table comparing diameter and length parameter of PTFE fibres and ropes based on a total of 100 measured fibrils. (d) Distribution of number of inter-windings in PTFE ropes.

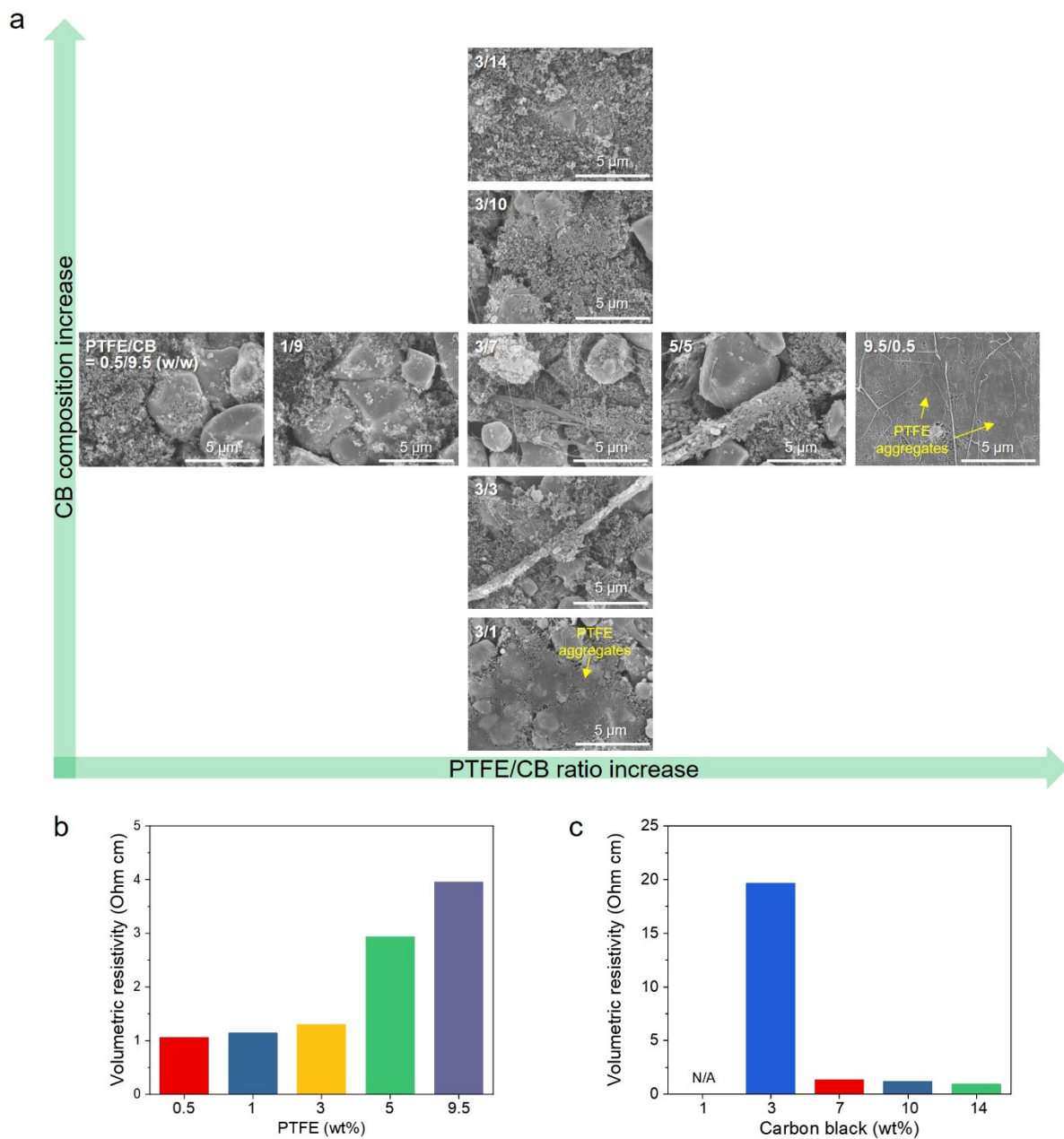


Figure S3. Optimizing weight ratio of PTFE and carbon black in DDE. (a) SEM images after 2nd kneading process for various ratios of PTFE and CB as a function of PTFE/CB ratio (horizontal axis) (A:B:C = 90 : x : 10 - x (w/w/w)) and carbon black composition at a fixed PTFE weight of 3 wt% (A:B:C = 90 : 3 : y (w/w/w)) (vertical axis). Volume resistivity of DDE after the roll pressing process corresponding to (b) PTFE/CB ratio and (c) carbon black composition.

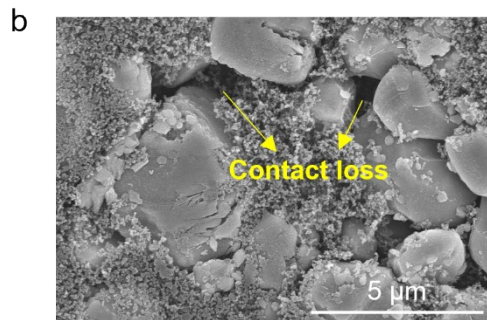
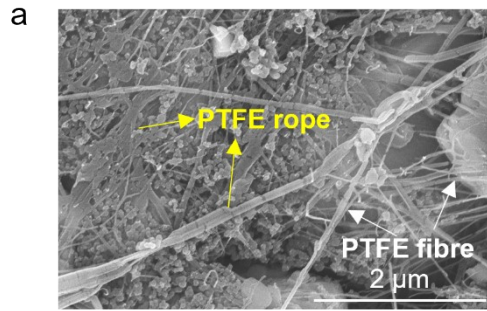


Figure S4. SEM images of (a) DDE and (b) SDE.

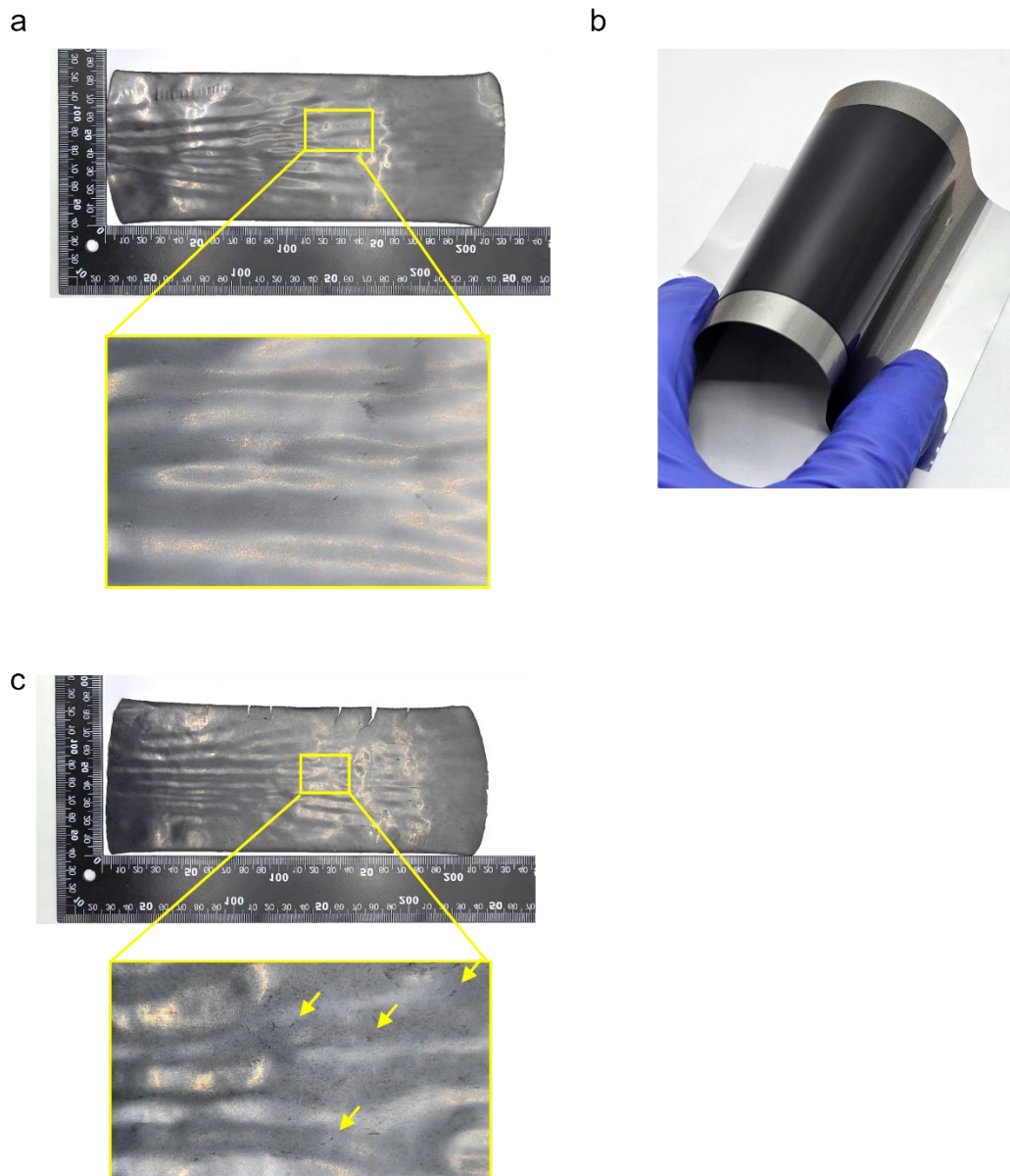


Figure S5. Photographs of DDE (a) after roll pressing and (b) lamination onto current collector. (c) Photograph of SDE after roll pressing. Yellow arrows indicate dark spot showing non-uniform distribution.

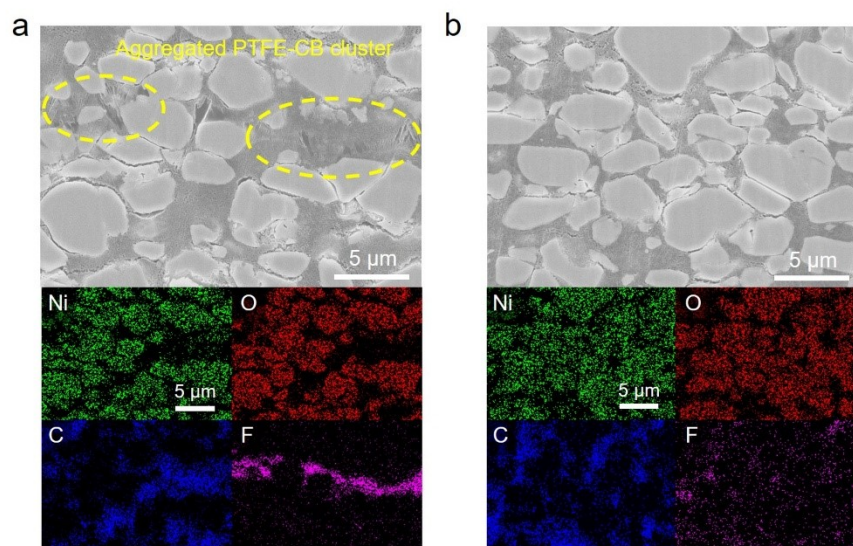


Figure S6. Ion-milled cross-sectional SEM images and corresponding EDS elemental mapping images of (a) SDE and (b) DDE.

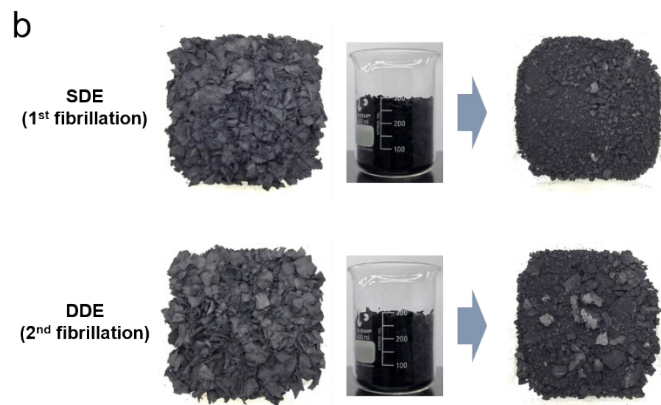
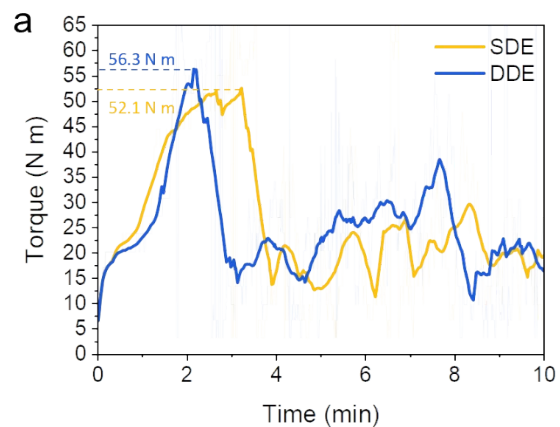


Figure S7. (a) Real-time measurement of the kneading torque change of SDE and DDE granules and (b) photographs of before and after the measurement.

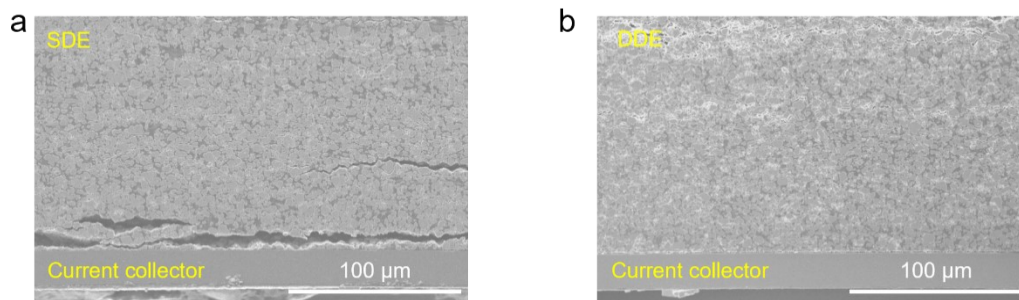


Figure S8. Ion-milled cross-sectional SEM images of (a) SDE and (b) DDE after lamination process.

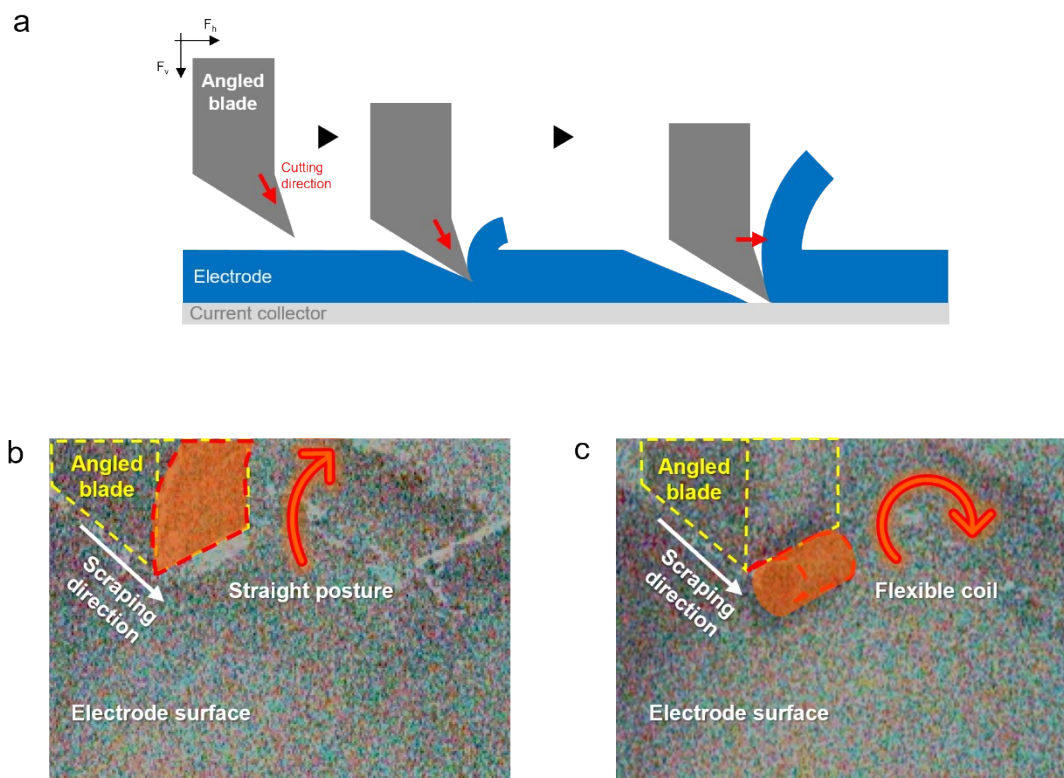


Figure S9. (a) Schematic representation of the SAICAS measurement. Snapshot of video clip showing the electrode scraping during SAICAS analysis featuring the difference between (b) SDE and (c) DDE.

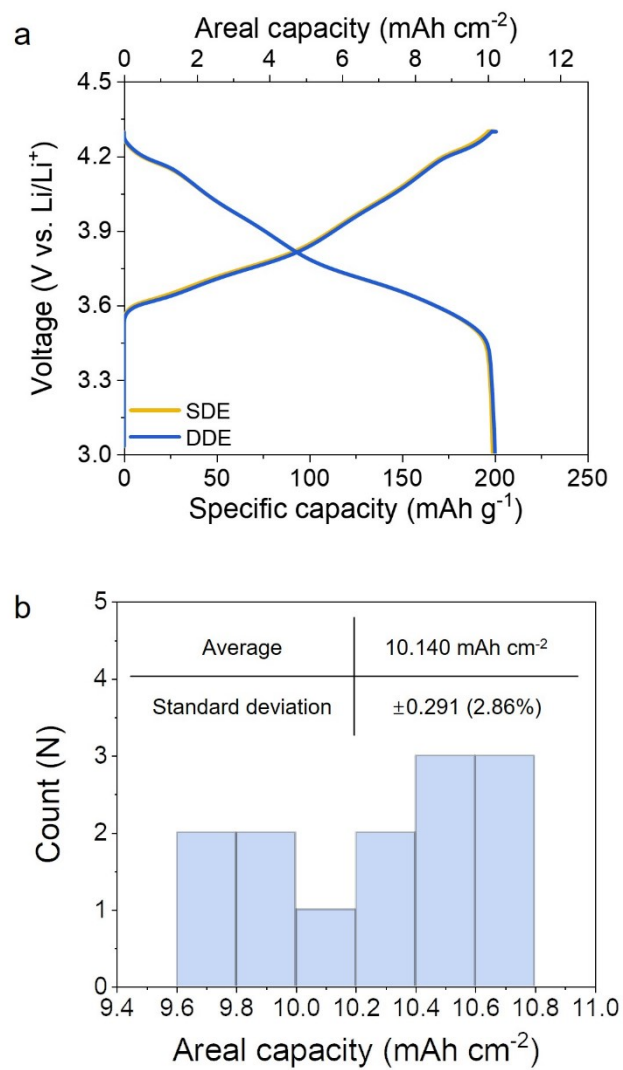


Figure S10 (a) Galvanostatic charge/discharge profile of SDE and DDE coin half cells under a voltage range of 3.0 – 4.3 V (vs. Li/Li⁺) at 0.1 C/0.1 C. (b) Areal capacity distribution of DDE coin half cells, demonstrating the uniformity of the electrodes.

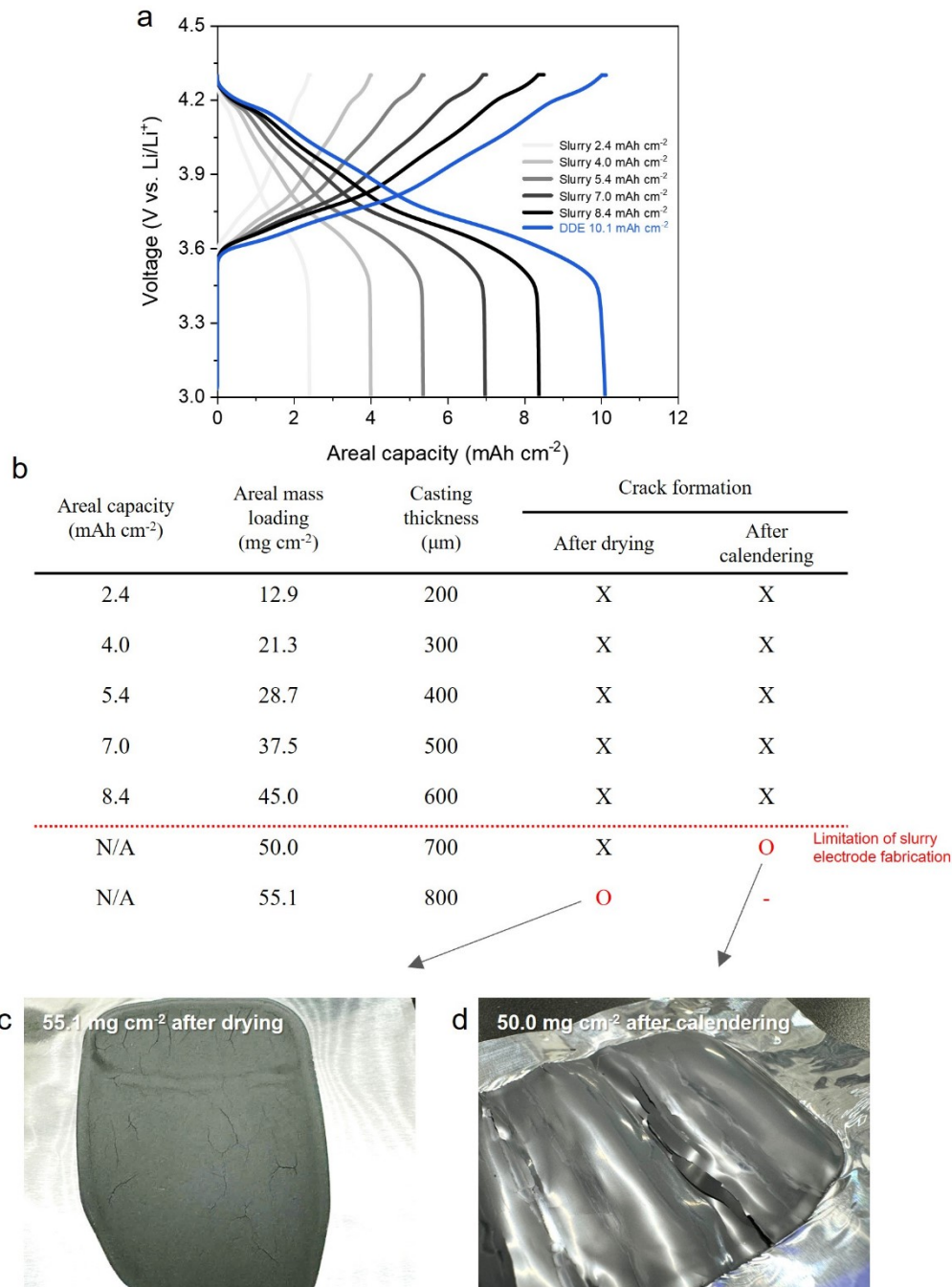


Figure S11 Comparison with conventional slurry electrode. (a) Galvanostatic charge/discharge voltage profiles of the DDE and conventional slurry electrode with varying areal mass loading. (b) Summary of fabrication details for slurry electrodes with varying areal mass loading. Photographs of the slurry electrode corresponding to (c) 55.1 mg cm⁻² after drying and (d) 50.0 mg cm⁻² after roll press.

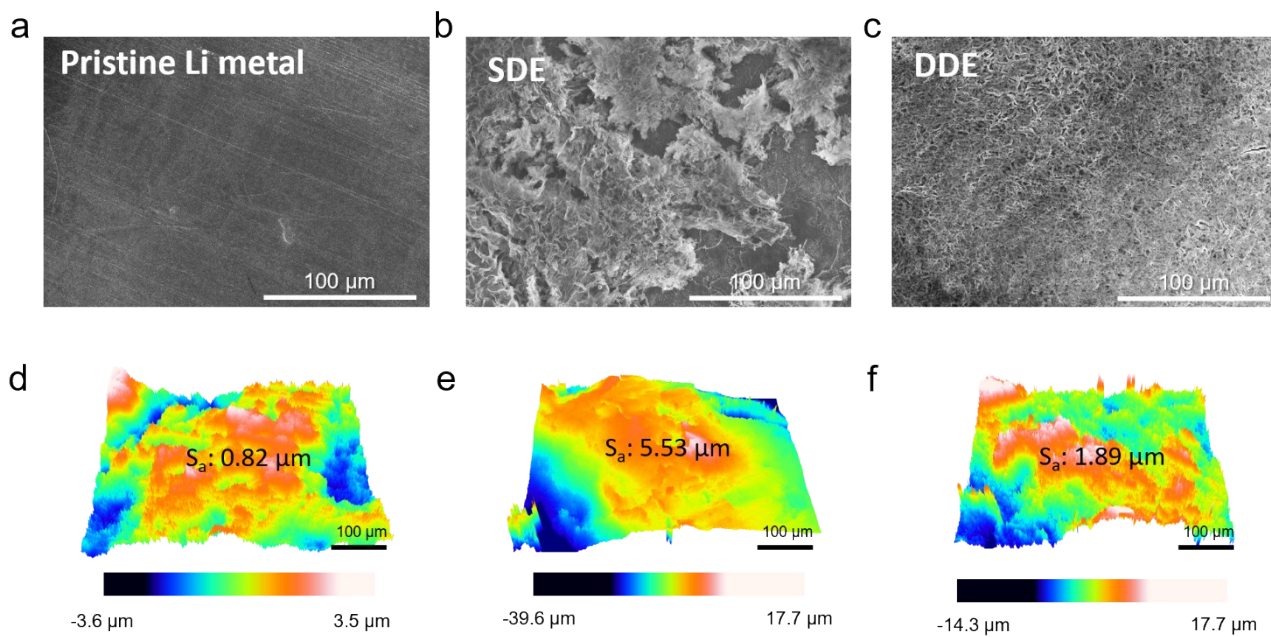


Figure S12 SEM images and surface topography of (a, d) pristine Li metal, and Li metal after 3 cycles paired with (b, e) the SDE and (c, f) the DDE

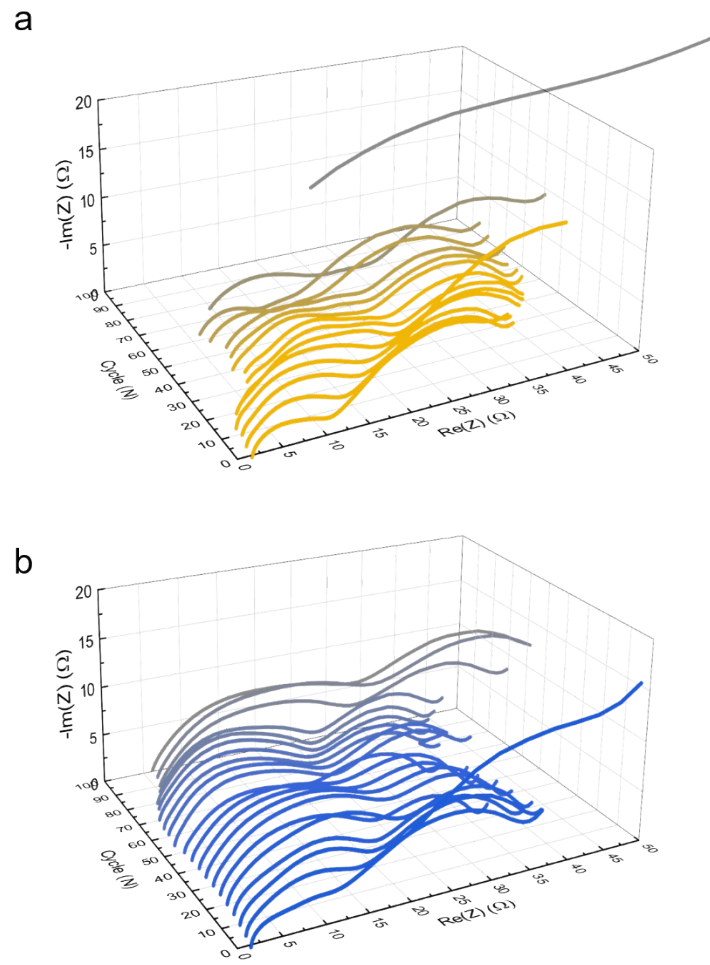


Figure S13 Nyquist plots of (a) SDE and (b) DDE as a function of the number of cycles.

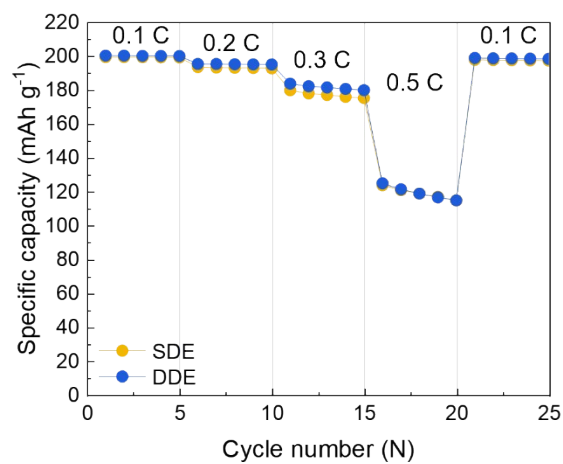


Figure S14. Discharge rate capability of SDE and DDE over a wide range of discharge current densities (0.1 –0.5 C) at a fixed charge current density of 0.1 C.

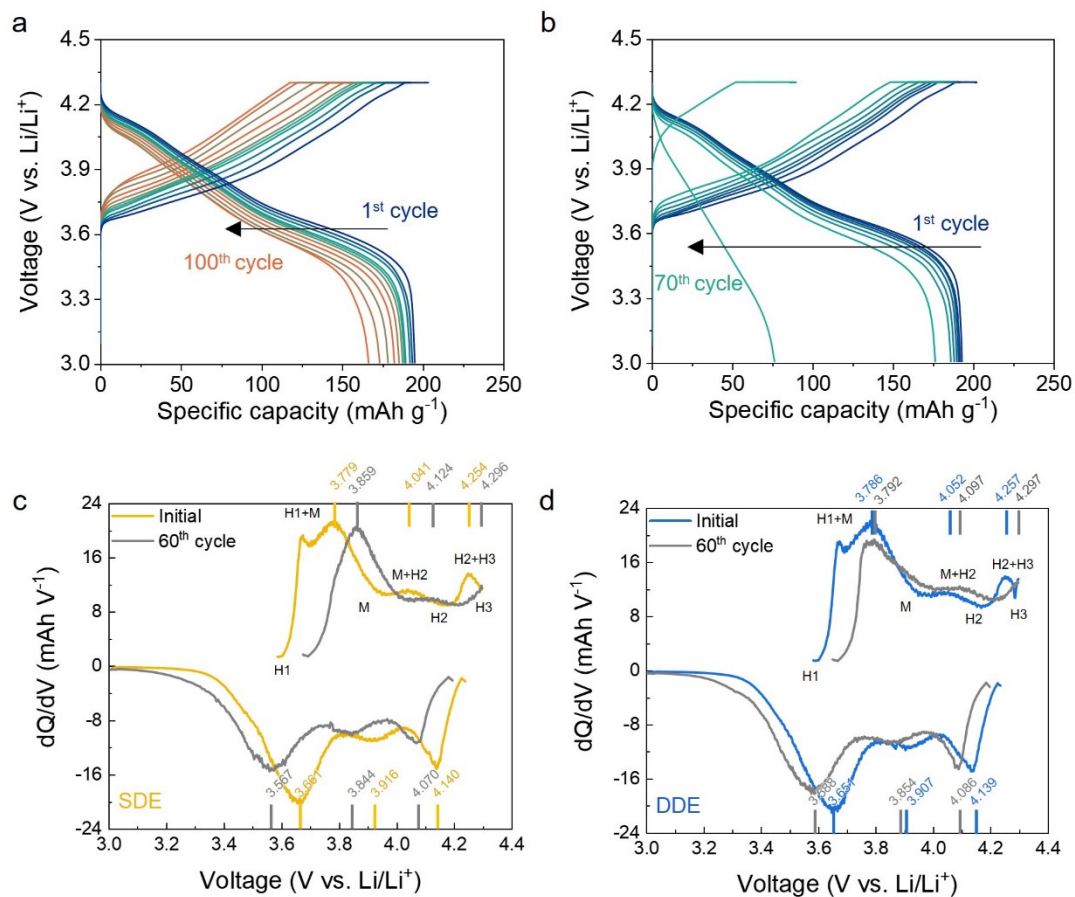


Figure S15 Galvanostatic charge/discharge profiles of (a) DDE and (b) SDE coin half cell at every 10 cycles at 0.2 C/0.2 C. Electrochemical profiles of differential capacities for the (c) SDE and (d) DDE at initial cycle and 60th cycle.

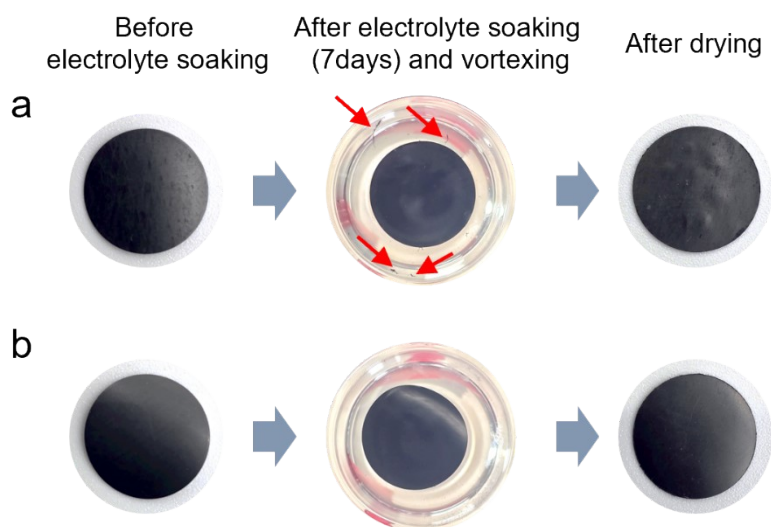


Figure S16 Electrolyte stability test of the (a) SDE and (b) DDE. Red arrows indicate partially broken electrodes from SDE after soaking and vortexing.

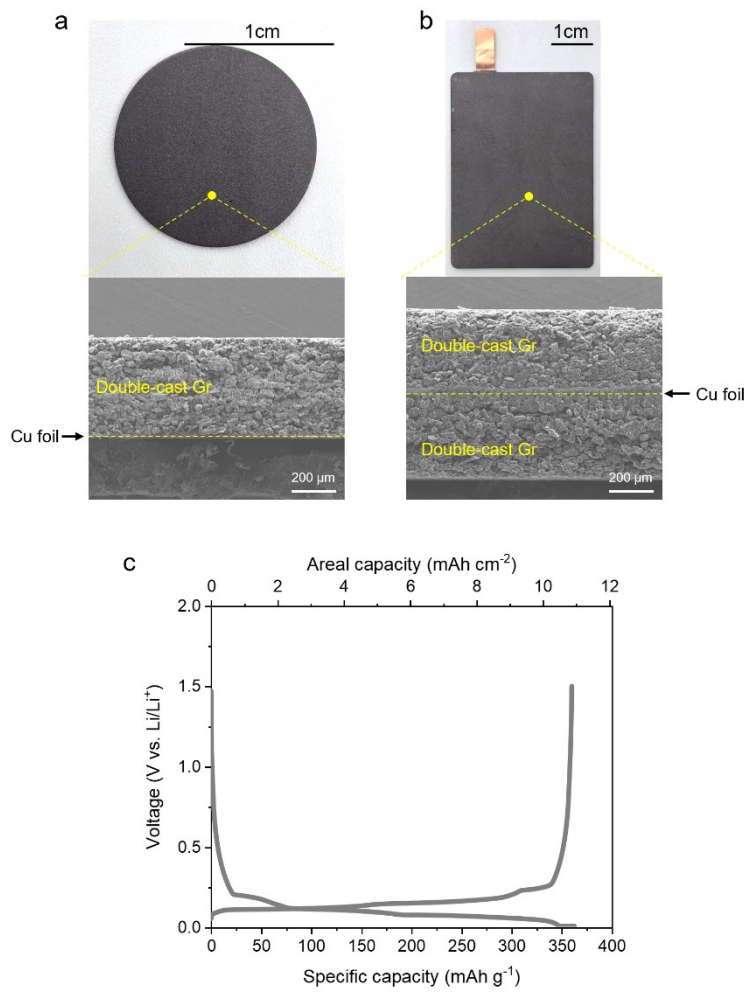


Figure S17. Photograph and corresponding cross-sectional SEM images of double-cast graphite anodes: (a) Single-side coating for coin cells and (b) double-side coating for pouch cells. (c) Galvanostatic charge/discharge profile of the double-cast graphite half cell under a voltage range of 0.005 – 1.5 V (vs. Li/Li⁺) at 0.1 C/0.1 C.

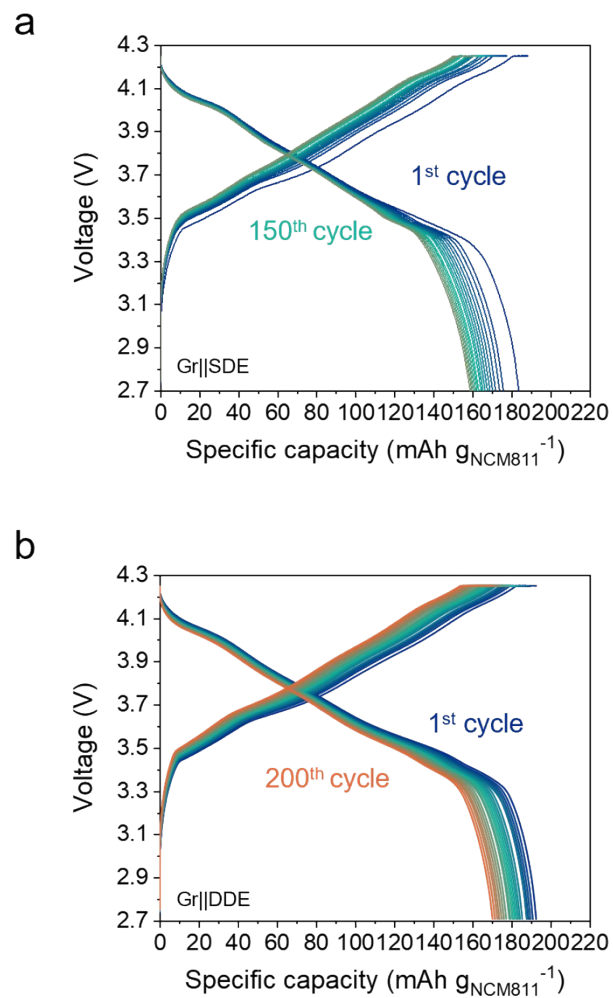


Figure S18. Galvanostatic charge/discharge profiles (a) Gr||SDE and (b) Gr||DDE full cells in potential window of 2.7 – 4.25 V at every 10 cycles.

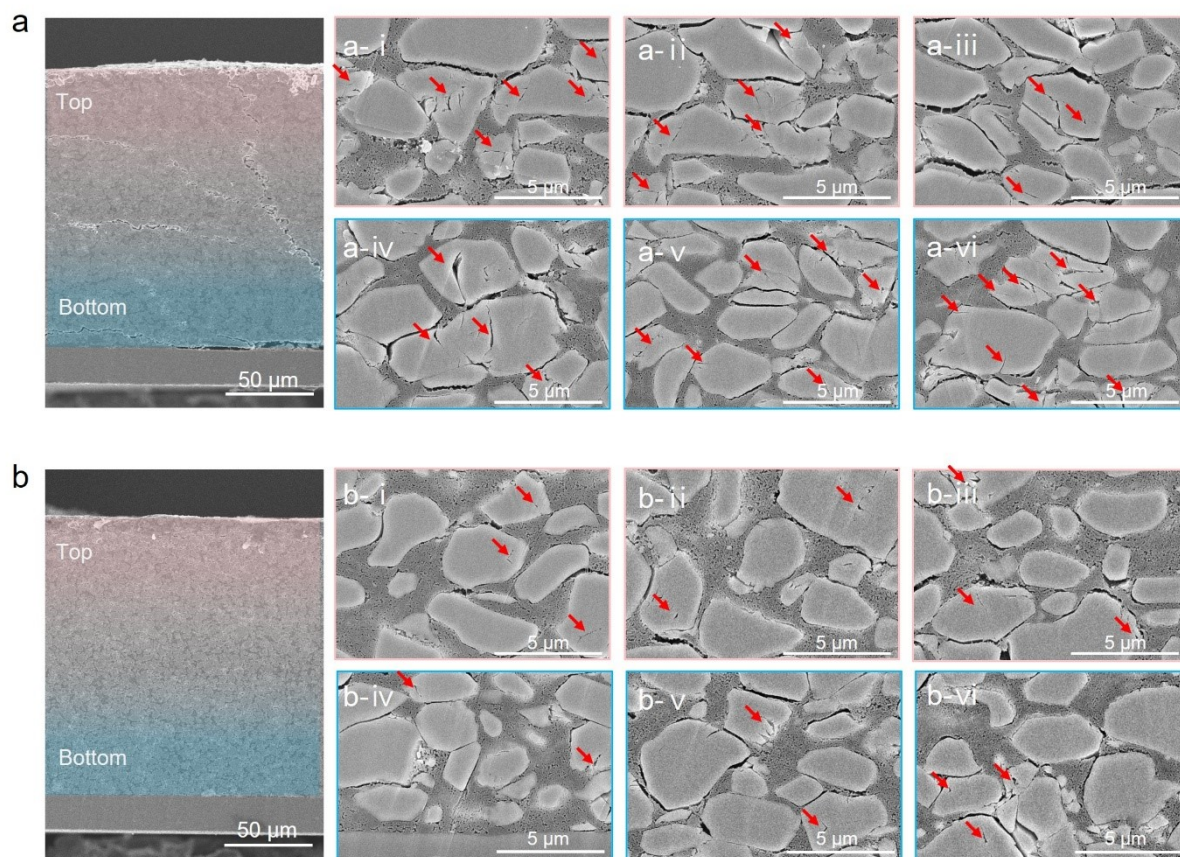


Figure S19. Cross-sectional SEM images of the electrodes after 50 cycles in half cells. Top views (a-i – iii) and bottom views (a-iv – vi) of SDE. Top views (b-i – iii) and bottom views (b-iv – vi) of DDE. (scale bars = 5 μm) The red arrows indicate particle cracks. The SDE exhibited larger and more numerous particle cracks compared to the DDE.

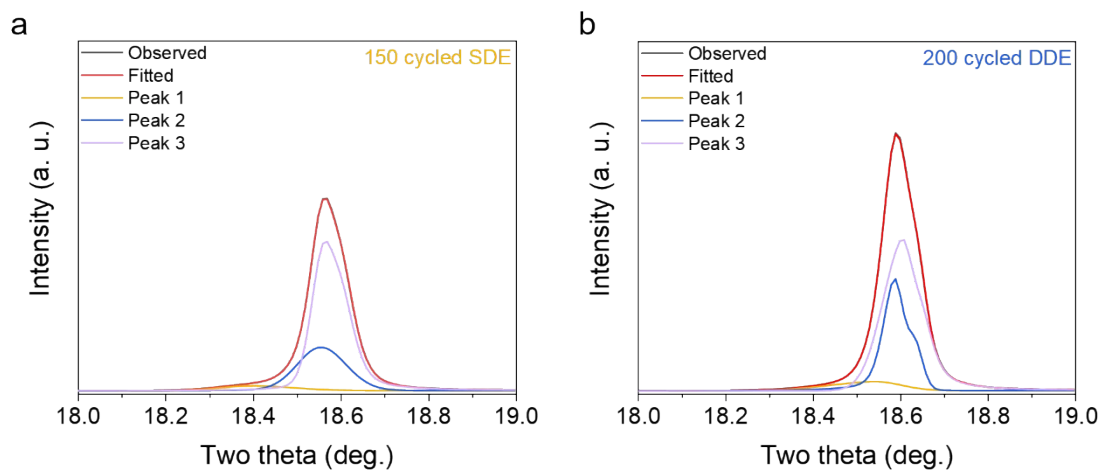


Figure S20. Peak deconvolution assigned to the (003) plane in XRD patterns of (a) SDE and (b) DDE cathodes after cycle, paired with Gr anode to confirm degree of heterogeneity by electrochemical degradation.

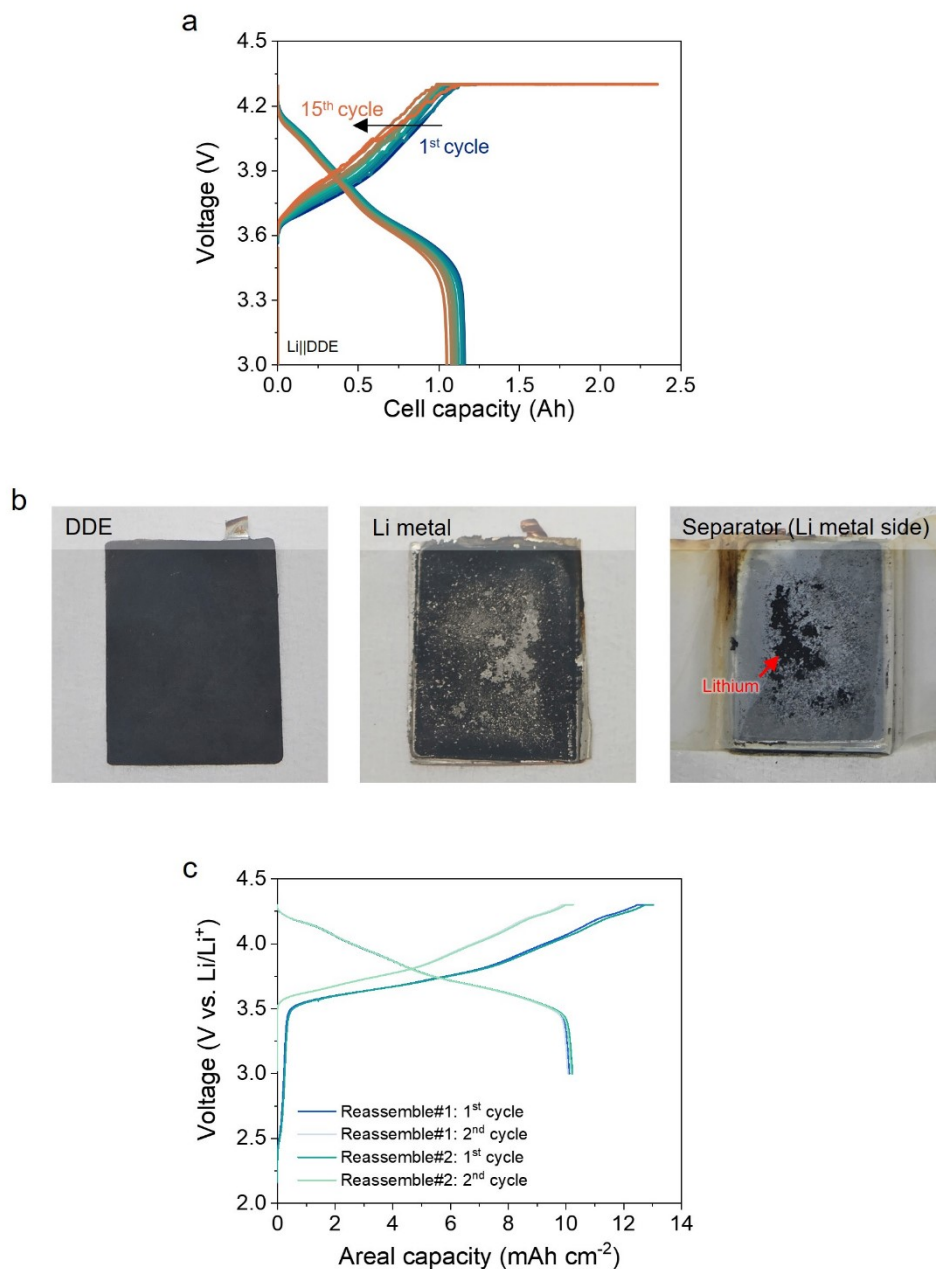


Figure S21. Galvanostatic charge/discharge profile of (a) Li||DDE pouch full cell and at 0.2 C/0.2 C in potential window of 2.75– 4.3 V (vs. Li/Li⁺). (b) Photographs of the disassembled DDE, Li metal, and separator of Li||DDE pouch full cell after 15 cycles. (c) Initial galvanostatic charge/discharge profiles of two reassembled DDE half coin cells at 0.05 C/0.05 C.

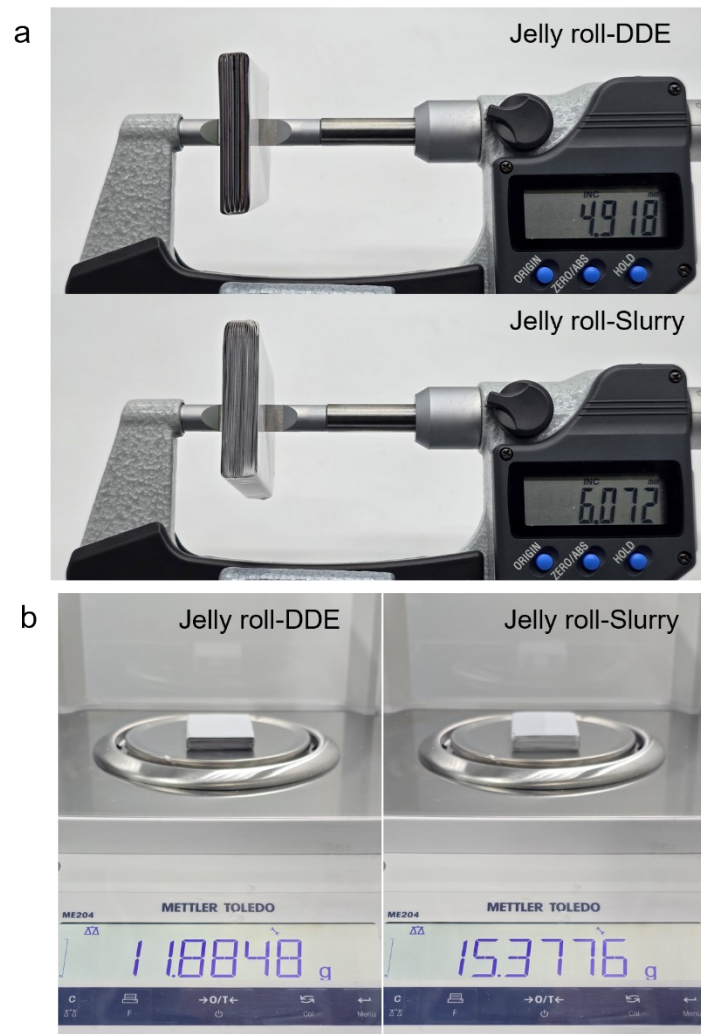


Figure S22. Comparison of (a) thickness and (b) mass of 1.2 Ah-class jelly roll composed of DDE and conventional slurry-based NCM811 cathode, paired with graphite anode.

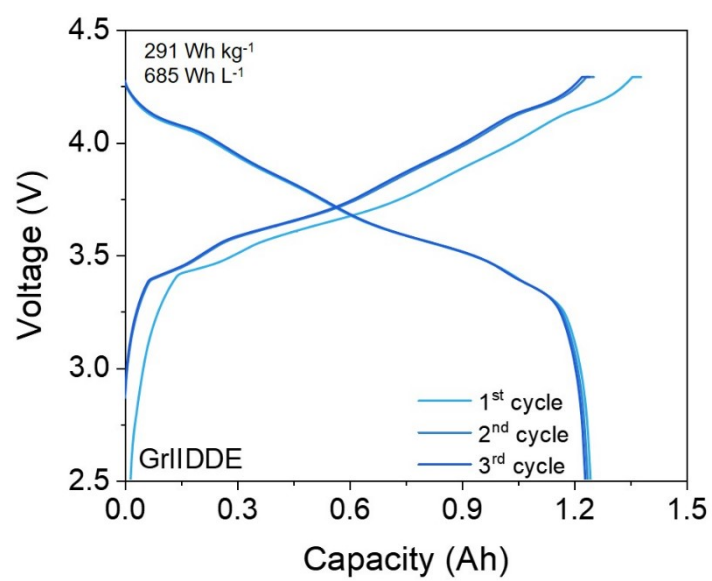


Figure S23. Galvanostatic charge/discharge profile of Gr||DDE pouch full cell for initial formation cycles in potential window of 2.5 – 4.29 V at 0.1 C/0.1 C.

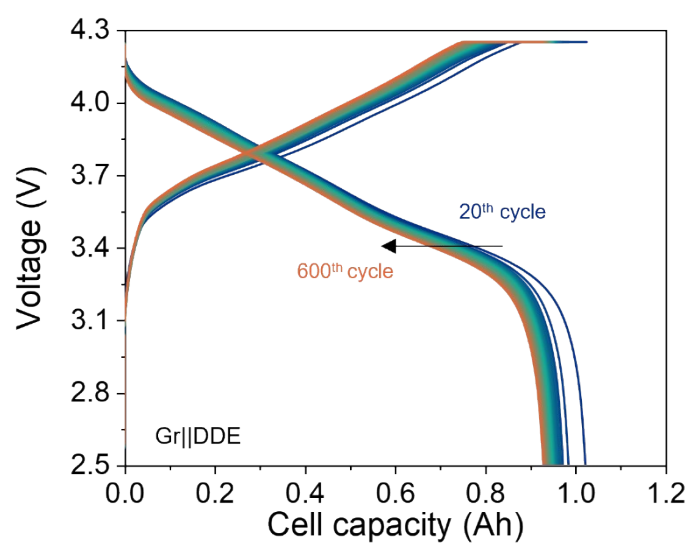


Figure S24. Galvanostatic charge/discharge profile of Gr||DDE pouch full cell at every 20 cycles in potential window of 2.5 – 4.25 V at 0.2 C/0.2 C.

Parameter		Gr DDE	Li DDE	Gr Slurry
Cathode	Active material content [%]	90	90	94
	Reversible capacity [mAh g ⁻¹]	201	201	200
	Active material mass loading [mg cm ⁻²]	50.25	50.25	16.00
	Area capacity [mAh cm ⁻²]	10.1	10.1	3.2
Anode	Active material	Natural graphite	Li metal	Natural graphite
	Active material content [%]	96	-	94
	Reversible capacity [mAh g ⁻¹]	361	-	360
	Active material mass loading [mg cm ⁻²]	30.18	-	9.81
	Area capacity [mAh cm ⁻²]	10.89	-	3.53
Pouch cell	Number of cathode layers [EA]	5	5	17
	Number of anode layers [EA]	6	6	18
	N/P ratio	1.08	-	1.10
	E/C ratio [g Ah ⁻¹]	3.2	3.2	3.2
	Double-sided cathode weight [g]	1.343	1.343	0.478
	Double-sided cathode thickness [μm]	370	370	156
	Double-sided anode weight [g]	0.821	0.254	0.36
	Double-sided anode thickness [μm]	442	212	160
	Separator thickness [μm]	20	20	20
	Pouch film thickness [μm]	153	153	153
	Cell weight [g]	15.78	13.46	20.50
	Cell thickness [mm]	5.09	4.45	6.31
	Initial discharge energy [Wh]	4.59	4.69	5.14
	Initial discharge capacity [Ah]	1.25	1.23	1.39
	Initial Coulombic efficiency [%]	90.20	92.13	83.80
Gravimetric energy density [Wh kg ⁻¹]	291	349	250	
Volumetric energy density [Wh L ⁻¹]	685	800	618	

Table S1. Parameter comparison of designed pouch full cells.

No	Cathode material	Anode material	Areal capacity (mAh cm ⁻²)	Energy Density (Wh kg _{cell} ⁻¹)	Cell Capacity (Ah)	Cycle retention (% @ cycles)	Cycles @ 80% retention	Reference
This work	NCM811	Graphite	10.1	251	1.2	80.2 @ 600	-	This work
		Lithium	10.1	349	1.2	Failure @ 15	N/A	
1	NCM811	Lithium	10	427	1	Failure @ 52	N/A	[49]
2	NCM811	Lithium	4	609	0.507	72 @ 95	36	[52]
3	LNMO	Graphite	5.2	258.7	0.266	87.3 @ 1700	-	[53]
4	NCM712	Lithium	5.89	360	0.2464	85 @ 100	110	[54]
5	Sulfur	Lithium	6	N/A	0.126	62 @ 40	15	[55]
6	NCM811	Graphite	4.7	N/A	0.0752	96 @ 150	-	[56]
7	LFP	Graphite	7.5	N/A	0.055	91.4 @ 20	-	[57]
8	NCM622	Graphite	3.3	N/A	0.045	82.1 @ 350 (1 C) 82.5 @ 300 (0.33 C)	-	[58]
9	LFP	Graphite	1.1	N/A	0.0285	80 @ 110	110	[59]

Table S2. Comparison of the DDE and previously reported dry electrode-based pouch full cells.

Reference	Binder	Fabrication method	Active material	Conductive agent	Composition (A/C/B = w/w/w)	Thickness (μm)	Areal mass loading (mg cm^{-2})	Areal capacity (mAh cm^{-2})	Tap density (g cc^{-1}) (or porosity)
This work	PTFE	Fibrillation	NCM811	CB	90/3/7	180	56.1	10.1	3.1
S1	PTFE	Fibrillation	NCM811	CB, G, CNT, KB	95.5/3/1.5	140 (260)*	-	10 (20)*	3.65
S2	PTFE	Fibrillation	NCA	CB	96/1.8/2.2	139	50	10	3.6
S3	PTFE	Fibrillation	LNMO	CNF	93/5/2	260	68	9.5	
S4	PTFE	Fibrillation	NCM811	VGCF	94/5/1	180	40	8.5	(13 %)
S5	PTFE	Fibrillation	NCM811	O-SWNT	96/2/2	-	40	-	3.2-3.4
S6	PTFE	Fibrillation	NCA@MWNT	-	99.6/0.4 (A@C/B)	-	40	-	3.6-4
S7	PTFE	Fibrillation	NCM811	SWNT	97.88/0.12/2	-	36	7	3.4
S8	PTFE	Fibrillation	LMR	KB	80/10/3	116	29	7.1	-
S9	PTFE	Fibrillation	LFP	CB	97/1/2	175	35	5.5	2.3
S10	PTFE	Fibrillation	LCO	CNT	98/1/1	140 (420)*	33.1 (101.4)*	5 (15)*	-
S11	PTFE	Fibrillation	NCM622	CB	92/5/3	-	27	4.8	-
S12	PTFE	Fibrillation	NCA	CNT(coating)	99.6/0/0.4	-	23	4.6	4
S13	PTFE	Fibrillation	NCMA	CB	96/2/2	-	20	-	3.6-3.8
S14	PTFE	Fibrillation	LNMO Graphite	CB CNT	96/2/2 97.7/0.8/1.5	N/A	15.43	4.8 5.2	N/A
S15	PTFE	Fibrillation	NCA	CB	85/1/1/13	-	15	N/A	3.19
S16	PTFE	Fibrillation	NCM900505	CNF/LPSCI	85/2/0.1/13	200	N/A	N/A	N/A
S17	PTFE	Fibrillation	ZnI ₂	AC	65/30/5 80/17/3	586	100	-	-
S18	PTFE	Fibrillation	Sulfur/Carbon (8/2 = w/w)	CB, MWNT	80/9.5/9.5/1	97	8	11.6	1.29
S19	PTFE	Fibrillation	Graphite	CB	96/1/3	92	14.4	4.8	1.55
S20	PTFE/PAA	Fibrillation	NCM811	CB	96.8/1.2/2	90	30	-	3.4
S21	PTFE/PVDF	Fibrillation	Graphite	CB	90/5/3/2	180	27	8.2	1.67
S22	PTFE/PVP	Fibrillation	Graphite	CNT	96/1/3	93	-	4.8	1.5
S23	PVDF	Electrostatic spray	NCM	CB	90/5/5	200	63	9.11	(20-25 %)
S24	PVDF	Electrostatic spray	NCM111	CB	90/5/5	59	N/A	2.4	N/A
S25	PVDF	Electrostatic spray	LCO	CB	80/10/10	50	N/A	N/A	N/A
S26	PVDF	Electrostatic spray	NCM523	CB	87.5/5/7.5	12	3	N/A	(35-40 %)
S27	PVDF	Electrostatic spray	NCM622	CB	90/5/5	N/A	N/A	N/A	(30-35 %)
S27	PVDF	Electrostatic spray	Graphite	CB	90/5/5	10	N/A	N/A	N/A
S28	PVDF	Electrostatic spray	Graphite	-	97/0/3	87	13.4	4.7	1.5
S29	PVDF	Electrostatic spray	Graphite	CB	92/2/6	35	4	N/A	N/A
S30	PVDF	Dry spray	LTO	CB	80/10/10	N/A	N/A	N/A	N/A
S31	PVDF	Planar press	NCM712	MWNT	80/15/5	573 221	100 31	17.6 5.3	-
S32	PVDF	Planar press	LFP	CB	80/10/10	N/A	5.24	N/A	N/A
S33	PVDF	Roll mill	NCM622	CB	93.5/2.5/3 (+ 1% graphite)	72	20.1	-	-
S34	Phenoxy resin	Planar press	NCM811	MWNT	95.5/1.5/3	150	40	-	2.14
S35	PEO/LiTFSI	Extrusion or Roll mill	LFP	CB	72.32/3.7/24	60	-	1.5	1.3-1.45
S36	h-Graphene	Planar press	LFP	-	1/1	160-340	11.6	-	-

* These studies achieved extremely high areal capacities ($> 15 \text{ mAh cm}^{-2}$), however, they used electrode with an areal capacity of $\sim 10 \text{ mAh cm}^{-2}$ as their main sample, due to several reasons such as the limited effectiveness of pouch cell energy density and performance comparison with slurry-based electrodes.

Table S3 Comparison of the DDE and previously reported various dry electrode strategies.

Supplementary reference

- S1. H. Oh, G.-S. Kim, J. Bang, S. Kim and K.-M. Jeong, *Energy & Environmental Science*, 2025, **18**, 645-658.
- S2. J. Kim, K. Park, M. Kim, H. Lee, J. Choi, H. B. Park, H. Kim, J. Jang, Y. H. Kim, T. Song and U. Paik, *Advanced Energy Materials*, 2024, **14**, 2303455.
- S3. W. Yao, M. Chouchane, W. Li, S. Bai, Z. Liu, L. Li, A. X. Chen, B. Sayahpour, R. Shimizu, G. Raghavendran, M. A. Schroeder, Y.-T. Chen, D. H. S. Tan, B. Sreenarayanan, C. K. Waters, A. Sichler, B. Gould, D. J. Kountz, D. J. Lipomi, M. Zhang and Y. S. Meng, *Energy & Environmental Science*, 2023, **16**, 1620-1630.
- S4. K. Raju, L. Wheatcroft, M. C. Lai, A. Mahadevegowda, L. F. J. Piper, C. Ducati, B. J. Inkson and M. De Volder, *Journal of The Electrochemical Society*, 2024, **171**, 080519.
- S5. H. Kim, J. H. Lim, T. Lee, J. An, H. Kim, H. Song, H. Lee, J. W. Choi and J. H. Kang, *Acs Energy Letters*, 2023, **8**, 3460-3466.
- S6. J. Shin, J. H. Lee, J. K. Seo, W. T. A. Ran, S. M. Hwang and Y. J. Kim, *International Journal of Energy Research*, 2022, **46**, 16061-16074.
- S7. I. Hwang, K. E. Sung, J. Hong, G. S. Kang and J. Yoon, *Chemical Engineering Journal*, 2025, **506**, 160159.
- S8. Z. Qu, Y. Wang, C. Zhang, S. Geng, Q. Xu, S. Wang, X. Zhao, X. Zhang, B. Yuan, Z. Ouyang and H. Sun, *Adv Mater*, 2025, **37**, e2410974.
- S9. K. Kwon, J. Kim, S. Han, J. Lee, H. Lee, J. Kwon, J. Lee, J. Seo, P. J. Kim, T. Song and J. Choi, *Small Sci*, 2024, **4**, 2300302.
- S10. T. J. Embleton, J. H. Choi, S.-J. Won, J. Ali, K. S. Saqib, K. Ko, M. Jo, J. Hwang, J. Park, J. H. Lee, J. Kim, M. K. Kim, J.-W. Jung, M. Park and P. Oh, *Energy Storage Materials*, 2024, **71**, 103542.
- S11. Z. Q. Wei, D. W. Kong, L. J. Quan, J. H. Huang, S. Chen, X. C. Cao, R. Q. Zhang, H. J. Liu, L. D. Xing and W. S. Li, *Energy Storage Materials*, 2025, **75**, 04071.
- S12. J. K. Koo, J. Lim, J. Shin, J. K. Seo, C. Ha, W. T. A. Ran, J.-H. Lee, Y. Kwon, Y. M. Lee and Y.-J. Kim, *Energy Storage Materials*, 2025, **78**, 104270.
- S13. S. Hong, J. K. Seo, C. Ha, S. M. Oh and Y. J. Kim, *Journal of Power Sources*, 2025, **638**, 236621.
- S14. Z. Wei, D. Kong, L. Quan, J. He, J. Liu, Z. Tang, S. Chen, Q. Cai, R. Zhang, H. Liu, K. Xu, L. Xing and W. Li, *Joule*, 2024, **8**, 1350-1363.
- S15. D. Shin, J. S. Nam, C. T. L. Nguyen, Y. Jo, K. Lee, S. M. Hwang and Y. J. Kim, *J Mater Chem A*, 2022, **10**, 23222-23231.
- S16. F. Hippauf, B. Schumm, S. Doerfler, H. Althues, S. Fujiki, T. Shiratsuchi, T. Tsujimura, Y. Aihara and S. Kaskel, *Energy Storage Materials*, 2019, **21**, 390-398.
- S17. H. Wu, S.-J. Zhang, J. Vongsvivut, M. Jaroniec, J. Hao and S.-Z. Qiao, *Joule*, 2025, DOI:

10.1016/j.joule.2025.102000, 102000.

S18. H. Sul, D. Lee and A. Manthiram, *Small*, 2024, **20**, e2400728.

S19. S. Han, E.-H. Noh, S. Chae, K. Kwon, J. Lee, J.-S. Woo, S. Park, J. W. Lee, P. J. Kim, T. Song, W.-J. Kwak and J. Choi, *Journal of Energy Storage*, 2024, **96**, 112693.

S20. K.-E. Sung, I. Hwang, J. Choi, S.-K. Jung and J. Yoon, *Chemical Engineering Journal*, 2025, **511**, 161789.

S21. Y. Zhang, S. Lu, F. Lou and Z. Yu, *Energy Technology*, 2022, **10**, 2200732.

S22. J. Lee, C. Y. Son, S. Han, S. Yang, P. J. Kim, D. Lee, J. W. Lee, W.-H. Ryu and J. Choi, *Chemical Engineering Journal*, 2025, **503**, 158271.

S23. J. Liu, B. Ludwig, Y. Liu, Z. Zheng, F. Wang, M. Tang, J. Wang, J. Wang, H. Pan and Y. Wang, *Advanced Materials Technologies*, 2017, **2**, 1700106.

S24. M. Wang, J. Hu, Y. Wang and Y.-T. Cheng, *Journal of The Electrochemical Society*, 2019, **166**, A2151-A2157.

S25. B. Ludwig, Z. Zheng, W. Shou, Y. Wang and H. Pan, *Scientific Reports*, 2016, **6**, 23150.

S26. E. Zhen, J. Jiang, C. Lv, X. Huang, H. Xu, H. Dou and X. Zhang, *Journal of Power Sources*, 2021, **515**, 230644.

S27. Y. Liu, X. Gong, C. Podder, F. Wang, Z. Li, J. Liu, J. Fu, X. Ma, P. Vanaphuti, R. Wang, A. Hitt, Y. Savsatli, Z. Yang, M. Ge, W.-K. Lee, B. Yonemoto, M. Tang, H. Pan and Y. Wang, *Joule*, 2023, **7**, 952-970.

S28. J. A. Barreras-Uruchurtu, N. Besnard, C. Paul, L. Marchal, S. Devisme and B. Lestriez, *Journal of The Electrochemical Society*, 2025, **172**, 020522.

S29. J. Liu, B. Ludwig, Y. Liu, H. Pan and Y. Wang, *ACS Applied Materials & Interfaces*, 2019, **11**, 25081-25089.

S30. D.-W. Park, N. A. Cañas, N. Wagner and K. A. Friedrich, *Journal of Power Sources*, 2016, **306**, 758-763.

S31. W. D. Connor, S. Arisetty, K. P. Yao, K. Fu, S. G. Advani and A. K. Prasad, *Journal of Power Sources*, 2022, **546**, 231972.

S32. M. Ryu, Y. K. Hong, S. Y. Lee and J. H. Park, *Nat Commun*, 2023, **14**, 1316.

S33. A. Gyulai, W. Bauer and H. Ehrenberg, *ACS Applied Energy Materials*, 2023, **6**, 5122-5134.

S34. H. M. Kim, B. I. Yoo, J. W. Yi, M. J. Choi and J. K. Yoo, *Nanomaterials (Basel)*, 2022, **12**, 3320.

S35. L. Helmers, L. Froböse, K. Friedrich, M. Steffens, D. Kern, P. Michalowski and A. Kwade, *Energy Technology*, 2021, **9**, 2000923.

S36. D. J. Kirsch, S. D. Lacey, Y. Kuang, G. Pastel, H. Xie, J. W. Connell, Y. Lin and L. Hu, *ACS Applied Energy Materials*, 2019, **2**, 2990-2997.